Chemical Engineering Science 90 (2013) 119–129

Contents lists available at SciVerse ScienceDirect

Chemical Engineering Science

journal homepage: www.elsevier.com/locate/ces

Effect of surface energy on the transition from fixed to bubbling gas-fluidised beds

Fang Yang, Colin Thornton*, Jonathan Seville [1]

School of Chemical Engineering, University of Birmingham, Birmingham B15 2 TT, UK

HIGHLIGHTS

- U_{mf} is an isostatic state that is the transition to fluid-like behaviour.
- The so-called 'homogeneous expansion' regime is not in fact homogeneous.
- The idea that bed expansion is due to the 'elasticity' of the bed is not tenable.

ARTICLE INFO

Article history:
Received 13 July 2012
Received in revised form
15 November 2012
Accepted 20 December 2012
Available online 28 December 2012

Keywords:
Powder technology
Fluidization
Granular materials
Simulation
Discrete element method
Homogeneous expansion

ABSTRACT

Two-dimensional DEM–CFD simulations have been performed in order to examine the effect of surface energy on the transitional behaviour from fixed bed to bubbling bed for Geldart Type A particles. The results of the simulations presented in the paper show that any effect of surface energy on the magnitude of U_{mf} is not due to increasing bed resistance as a result of increasing the interparticle bond strength. It is demonstrated that U_{mf} corresponds to a deterministic (isostatic) state that is in effect the initiation of the transition from solid-like to fluid-like behaviour. It is also shown that the so-called 'homogeneous expansion' regime is not in fact homogeneous. This is because the system, when $U > U_{mf}$, consists of agglomerates. Consequently, the idea that bed expansion is due to the 'elasticity' of the bed is not tenable. In order to break up the agglomerates and create a fully fluidised bed that will allow bubbling to occur, higher superficial gas velocities are required for higher values of surface energy. Once the bed is fully fluidised and bubbling occurs the effect of surface energy becomes insignificant.

1. Introduction

Many industrial chemical manufacturing processes rely on obtaining intimate contact between a gas and a solid. Frequently the most effective way of doing this is by fluidising the solids with a gas. For optimal reactor performance, and particularly in the manufacture of some ultrafine high technology materials such as silicon carbide and titania, it is attractive to use as small as possible a particle size, giving high surface area per unit volume. However, there is a limit to such reduction in size, caused by the increased effects of van der Waals forces at small particle diameters, which effectively make it impossible to fluidise particles below a few tens of micrometres in size.

The behaviour of fluidised solids falls into four more-or-less distinct categories, as first pointed out by Geldart (1973). Leaving aside large, dense particles whose behaviour is dominated by inertia (Geldart's Group D) the differences between the remaining three groups depend on the ratio of the adhesive force to the single particle weight (Molerus, 1982; Seville et al., 2000). If the adhesive force is much greater than the particle weight, fluidisation is impossible (Group C—cohesive) while if the opposite is true fluidisation is unaffected (Group B—bubbling). Particularly interesting behaviour occurs for particles for which the interparticle forces are comparable with the particle weight (Group A—aeratable). Such particle beds show a tendency to expand, apparently homogeneously, when gas is passed through them above the minimum fluidising velocity, U_{mf}. This distinguishes them from beds of larger particles that show bubbling behaviour for gas velocities immediately above U_{mf}. It was shown theoretically very early in the study of fluidisation (Jackson, 1963) that an expanded bed of particles in a gas should be unstable to voidage perturbations. Explanations for the stability of this expanded non-bubbling bed include internal 'elasticity' of the particle phase (Rietema, 1973; Rietema et al., 1993), stabilisation of internal voids (Donsi and Massimilla, 1973) and hydrodynamic effects (Foscolo and Gibilaro, 1984). However, the matter remains unresolved and expressions for the expansion behaviour and the

* Corresponding author. Tel.: +44 1926 402919.
E-mail address: c.thornton@bham.ac.uk (C. Thornton).
[1] Present address: Department of Chemical & Process Engineering, University of Surrey, Guildford, Surrey GU2 7XH, UK.

0009-2509
http://dx.doi.org/10.1016/j.ces.2012.12.034

maximum expansion beyond which bubbling occurs remain empirical; for example the most commonly used correlation for minimum bubbling velocity remains that of Abrahamsen and Geldart (1980)

There have been many experimental studies that have yielded much information about fluidised bed behaviour leading to many empirical correlations, but understanding of the fundamental mechanisms has been limited by the lack of suitable investigative techniques. Computer modelling of fluidised beds using two-fluid models in which both the gas and solid phases are modelled as continuous and fully interpenetrating has been employed to try to provide a more scientific understanding of fluidisation. Such modelling does not take account of the discrete nature of the solid phase and, although particle size and shape are notionally factored into the continuum representation of the solid phase, the degree of empiricism involved leaves a basic scientific interpretation of the results obtained from these models open to question. Relevant particle properties and interaction parameters that might be expected to affect the fluidisation characteristics of powders (elasticity, plasticity, interface properties) cannot be incorporated into these models in a direct manner.

The increasing power of computer hardware has made a Lagrangian-Eulerian modelling of gas-solid fluidisation feasible following the original work of Tsuji et al. (1993) who combined Discrete Element Method (DEM) modelling of the particle phase with Computational Fluid Dynamics (CFD) modelling of the fluid phase to simulate fluidised beds in 2D. This combined DEM–CFD approach makes it possible to incorporate material properties directly into the model and obtain a rational understanding of their effect on the fluidisation characteristics of powders. A distinct disadvantage of the discrete particle-continuum fluid model is the limited number of particles that can be handled and the small time-step dictated by the particle properties. Most applications to fluidised beds have been restricted to 2D simulations (Tsuji et al., 1993; Hoomans et al., 1996; Xu and Yu, 1997; Kaneko et al., 1999; Helland et al., 2000; Yuu et al., 2001; Rhodes et al., 2001b; Kafui et al., 2002; Di Renzo and Di Maio, 2007). Pseudo-3D simulations in which the discrete particle phase is modelled in 3D and the continuum fluid phase in 2D were reported by Kawaguchi et al. (2000). Fully-3D simulations in which both the particle fluid phases are modelled in 3D have been reported by Thornton and Kafui (2002), Takeuchi et al. (2004), Tsuji et al. (2008), Hilton et al. (2010), Kafui et al. (2011).

Three dimensional DEM–CFD simulations are extremely demanding in terms of computer time, primarily due to the much larger number of particles required compared to 2D simulations. The work reported in this paper was part of a PhD project and consequently, due to time constraints, it was elected to perform 2D simulations. It is expected that such simulations capture the physical basis of the observed phenomena, without, of course, matching the quantitative effects. The paper reports results of gas-solid fluidised bed simulations that illustrate the effect of surface energy on the behaviour of Geldart Group A type particle beds. Previous DEM–CFD studies of the effect of interparticle adhesive forces have been reported by Rhodes et al. (2001a), Xu et al. (2001), Ye et al. (2004), Pandit et al. (2006) and Moreno-Atanasio et al. (2007), all of whom used 2D simulations.

2. Simulation details

A series of 2D simulations was carried out using a container of height = 15.5 mm, width = 2 mm and thickness = 0.055 mm. The whole container is divided into small computational fluid cells, the size of which is $5d_p \times 5d_p$, where d_p is the mean particle diameter. The bed width corresponds to 40 times the mean particle diameter. Pressure is recorded for each fluid cell and the pressure difference between the bottom layer of cells and the layer of cells at the top of the container is taken as the pressure drop across the bed ΔP. The input parameters used for the gas phase and the particle phase are given in Tables 1 and 2 respectively and the particle size distribution is provided in Fig. 1 in terms of both the mass fraction and the number fraction.

Table 1
Gas phase input parameters.

Average gas molar mass	2.88E − 2 kg/mol
Gas viscosity	1.8E − 5 kg/m s
Gas density	1.1979 kg/m^3
Gas pressure (atmospheric)	101.3 kPa
Gas temperature	293 K

Table 2
Particle phase input parameters.

Particle size	45, 47.5, 50, 52.5, 55 μm
Mean particle size	50 μm
Number of particles	5000
Young's modulus	700 MPa
Particle density	2500 kg/m^3
Poisson's ratio	0.33
Friction coefficient	0.30

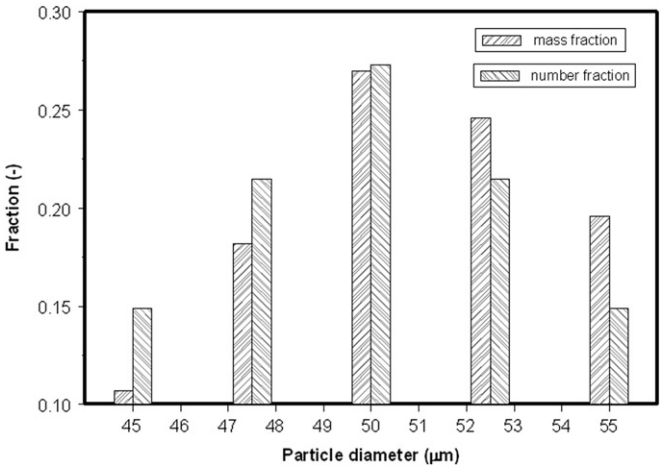

Fig. 1. Particle size distribution in terms of both mass and number fraction.

All the particles are initially randomly generated as a granular gas (no contacts) in a domain slightly smaller than the bed container. In the 2D simulations reported, all particle centres are located in the same plane and subsequent out of plane motion is suppressed. A vertical gravity field is then introduced in order to create a pluvially deposited bed of particles.

DEM simulations provide both qualitative and quantitative data. The qualitative information takes the form of computer visualisations, including video sequences, of particle locations, particle velocity distributions, fluid velocity distributions and particle–particle contact distributions. Quantitative information includes bed height, pressure drop and bed voidage as defined below.

The bed height used in the 2D simulations is defined in the following way, as shown in Fig. 2. First, the fluidised bed is divided into eight vertical columns. For each column, the topmost particle is identified and the highest computational fluid cell in which the topmost particle resides is recorded at the same time. The average height for each column is computed by accumulating all of the heights of particles in each of the highest computational

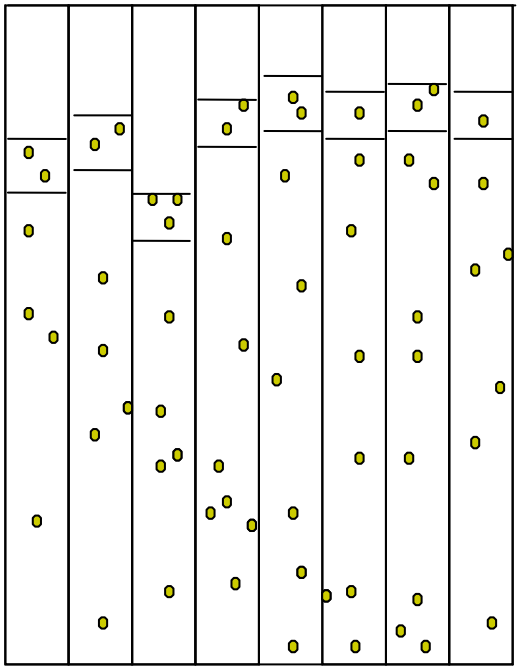

Fig. 2. Definition of bed height.

fluid cells and then calculating the average value. Finally, with the mass of the particles in each highest cell as the weighting parameter, the whole bed height is then calculated by taking the average of all the average column heights.

The fractional change in bed height ΔH^* and the normalised bed pressure drop ΔP^* are defined as

$$\Delta H^* = \frac{H - H_0}{H_0} \tag{1}$$

and

$$\Delta P^* = \frac{\Delta P}{gM/A} \tag{2}$$

where

$$M = \frac{\pi}{6}\sum_{N} \rho_p d_p^3 \tag{3}$$

and H_0 is the height of the initial packed bed, M is the total mass of the N particles, ρ_p and d_p are the solid density and average particle diameter, g is the acceleration due to gravity and A is the cross sectional area of the bed. In the 2D simulations, the depth of the bed is simply considered as one mean particle diameter. Based on this simplification, for the 2 mm wide shallow 2D bed, $A = 1.10^{-7}$ m^2 and the bed weight per unit area is 81.15 Pa. The overall voidage of the bed is defined as

$$\varepsilon = 1 - \frac{\sum_{i=1}^{N} V_i}{AH} \tag{4}$$

where A is the cross sectional area of the bed, H is the bed height, as defined above, and V_i is the volume of particle i.

The DEM–CFD modelling technique used has been fully described by Kafui et al. (2002) in which it was referred to as the PGF model. The model is essentially the same as that used by Tsuji's group except that the drag force is calculated using the Di Felice (1994) correlation since this provides a smooth continuous variation in drag force with voidage. A significant difference is that the detailed solid–solid interaction rules used to calculate the interparticle forces are based on theoretically and experimentally established contact mechanics. In order to model autoadhesive particle–particle interactions due to surface energy the normal contact interaction algorithms are based on the JKR model of adhesion (Johnson et al., 1971). Details of the theoretical basis for both the normal and tangential contact interaction rules can be found in Thornton and Yin (1991). In the JKR model of adhesive, elastic particle interactions, the maximum tensile force required to break a contact (the pull-off force) is given as

$$P_c = 3\gamma\pi R^* \; with \; \frac{1}{R^*} = \frac{1}{R_1} + \frac{1}{R_2} \tag{5}$$

where γ is the surface energy (assuming like spheres), and R_1 and R_2 are the radii of the two contacting particles. Consequently, in order to examine the effect of surface energy, values of γ were selected to make the average bond strength a multiple of the average particle weight

$$< P_c > = K < \mathrm{mg} > \tag{6}$$

As indicated by Eq. (5), for a given value of surface energy γ there will be, for a polydisperse system, a range of pull-off forces P_c depending on the radii of the two particles in contact. If a value of surface energy is specified that will give a value of $K=1$ for contact between two average sized spheres then the ranges of pull-off forces and K values for the range of contacts between different-sized spheres are shown in Tables 3 and 4. Note that, when $K=1$, the surface energy between two average sized spheresis 13.625 μJ/m^2 and accordingly the pull-off force $P_c = 1.605$ nN.

Table 3
Pull-off force (in nN) between two different sized spheres when the surface energy is 13.625 μJ/m^2.

	45.0 μm	47.5 μm	50.0 μm	52.5 μm	55.0 μm
45.0 μm	1.445	1.484	1.520	1.556	1.589
47.5 μm	1.484	1.524	1.564	1.601	1.637
50.0 μm	1.520	1.564	1.605	1.644	1.682
52.5 μm	1.556	1.601	1.644	1.685	1.725
55.0 μm	1.589	1.637	1.682	1.725	1.766

Table 4
K values between two different sized spheres when the surface energy is 13.625 μJ/m^2.

	45.0 μm	47.5 μm	50.0 μm	52.5 μm	55.0 μm
45.0 μm	1.235	1.078	0.935	0.837	0.744
47.5 μm	1.078	1.108	0.974	0.862	0.766
50.0 μm	0.935	0.974	1.000	0.885	0.787
52.5 μm	0.837	0.862	0.885	0.907	0.808
55.0 μm	0.744	0.766	0.787	0.808	0.827

3. Results

The initial pluvially deposited bed has a height of 6.539 mm with an initial voidage of 0.459 and 8465 interparticle contacts. An initial superficial gas velocity of 0.3 mm/s (more than an order of magnitude less than the minimum required for fluidisation) was introduced at the bottom of the bed and then increased incrementally. Throughout the simulations the pressure drop across the bed, the bed height, average bed voidage and the number of interparticle contacts were continuously monitored and, for each gas velocity increment, the time-averaged values were calculated. Fig. 3 shows the normalised pressure drop ΔP^*, the fractional change in bed height ΔH^* and the number of

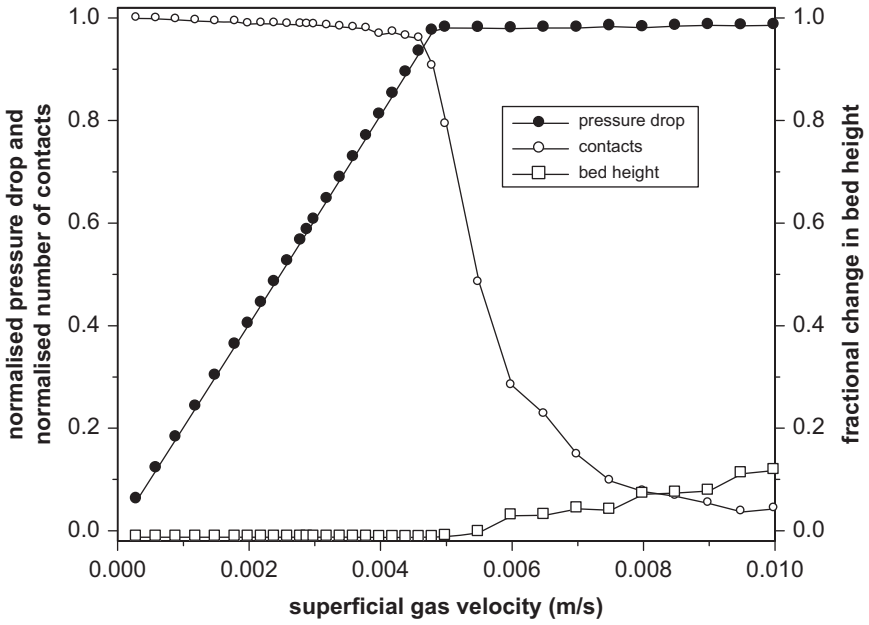

Fig. 3. Evolution of the normalised pressure drop, normalised number of contacts and fractional change in bed height with increase in superficial gas velocity.

contacts normalised by dividing by the initial number of contacts, all plotted against the superficial gas velocity U. In the fixed bed regime, the average bed voidage is constant since there is no change in the bed height, as indicating in Fig. 3.

For a fixed bed, the pressure gradient can be related to the gas velocity by the following correlation due to Ergun (1952)

$$\frac{\Delta P}{H} = 150\frac{(1-\varepsilon)^2}{\varepsilon^3}\frac{\mu U}{d_p^2} + 1.75\frac{(1-\varepsilon)}{\varepsilon^3}\frac{\rho_g U^2}{d_p} \tag{7}$$

In Fig. 3 it can be seen that the relationship between the pressure drop and the gas velocity is linear. This indicates that the second term on the RHS of Eq. (7) is insignificant due to the negligible inertia associated with such small-sized particles. When the pressure drop becomes equal to the bed weight divided by the cross-sectional area of the bed fluctuations in the pressure drop occur but the average pressure drop remains constant. Conventionally (see, for example, Geldart, 1986), the point where the average pressure drop first becomes equal to the bed weight divided by the cross sectional area of the bed is defined as 'minimum fluidisation' and the gas velocity at which this occurs is denoted by U_{mf}. This corresponds to a transition to what is conventionally referred to as 'homogeneous fluidisation' during which the bed expands, as can be seen in Fig. 3. At U_{mf}, the pressure gradient may be written as

$$\frac{\Delta P}{H} = (1-\varepsilon_{mf})\left(\rho_p - \rho_g\right)g \tag{8}$$

Ignoring the inertia term in Eq. (7) and equating Eqs. (7) and (8) the minimum fluidisation velocity can be calculated from

$$U_{mf} = \frac{g d_p^2\left(\rho_p - \rho_g\right)\varepsilon_{mf}^3}{150\mu(1-\varepsilon_{mf})} \tag{9}$$

The figure indicates that U_{mf}=0.0048 m/s which is 17% greater than the value of 0.0041 m/s predicted by Eq. (9). This difference may be due to the fact that these are 2D simulations, in contrast to the 3D experiments on which Eq. (7) was based. If U_{mf}= 0.0048 m/s is substituted into Eq. (9) then the corresponding coefficient is 127 rather than 150. The data in Fig. 3 were replotted as a graph of the pressure gradient $\Delta P/H$ against U (not shown). From the initial linear relationship the slope was found to be 2.52 MPa s/m^2. Substituting this value into Eq. (7) gives a coefficient of 116, corresponding to U_{mf}=0.0053 m/s. It is noted that the value of 0.0048 m/s, as indicated by Fig. 3, is approximately the average of the two predictions of 0.0041 m/s and 0.0053 m/s.

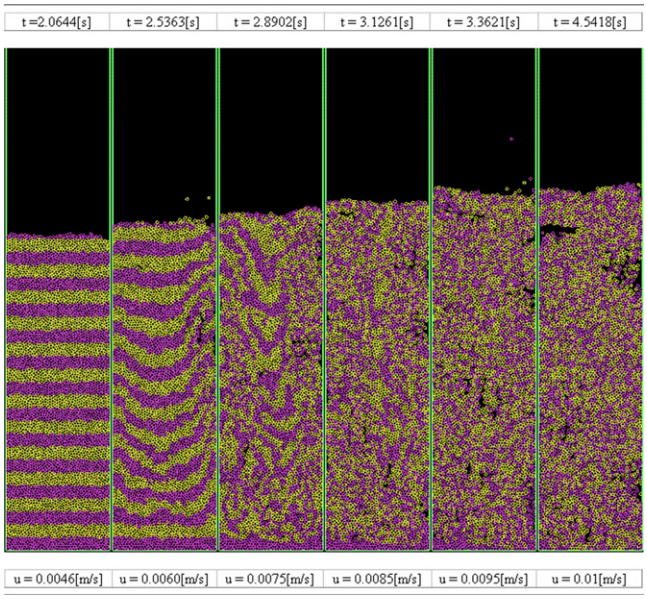

Fig. 4. Sequential snapshots of bed expansion with increasing gas velocity (K=0).

In Fig. 3 we also plot, for each gas velocity, the average number of interparticle contacts, normalised by the initial number of contacts. It can be seen that, at U_{mf}, about 10% of the original contacts have been lost. As the gas velocity is further increased the number of contacts decreases rapidly (70% of contacts have been broken at U=0.006 m/s) but then tends towards an asymptotic value of the order of 5% of the original number of contacts at U=0.01 m/s. This trend was also reported for 2D simulations of Geldart Group D particle beds by Kafui et al. (2002). The figure suggests that, during 'homogeneous fluidisation', there is a range of gas velocities over which the bed evolves from incipient fluidisation to a fully fluidised state.

The 'homogeneous' expansion behaviour can be visualised from the sequential snapshots of bed expansion shown in Figs. 4 and 5, for $K=0$ and $K=1$ respectively. For zero surface energy, $K=0$, no bubbles are observed before $U=0.0095$ m/s but bubbles start to appear around $U=0.01$ m/s. Although the bubble shown in Fig. 4 may not be fully developed it nevertheless indicates the onset of bubbling in the bed. This was confirmed when the gas velocity was incrementally increased to $U=0.02$ m/s and more obvious and larger bubbles were observed.

On this basis, U_{mb} is estimated to be 0.01 m/s for the case of zero surface energy. Fig. 5 shows that when $K=1$ and $U=0.01$ m/s there are no bubbles but that the increase in voidage resulting from the bed expansion takes the form of elongated narrow voids aligned in the vertical and horizontal directions, which occasionally are combined to form a cruciform shape. Similar observations were made by Donsi and Massimilla (1973) by direct observation of Group A particles through the transparent walls of their fluidised bed apparatus.

Fig. 6 provides comparisons between typical snapshots of the particle configurations for different surface energies when the superficial gas velocity is 0.01 m/s and 0.02 m/s. When $K=1$ and $K=2$ the figure shows that, with a gas velocity $U=0.01$ m/s, the bed has expanded without any obvious bubble observed. The figure also shows that, for $K=5$, channelling occurs when $U=0.01$ m/s. However, when the gas velocity is increased to $U=0.02$ m/s, fully developed bubbles are observed in all cases. This suggests that for $0 \leq K \leq 5$ the minimum bubbling velocity

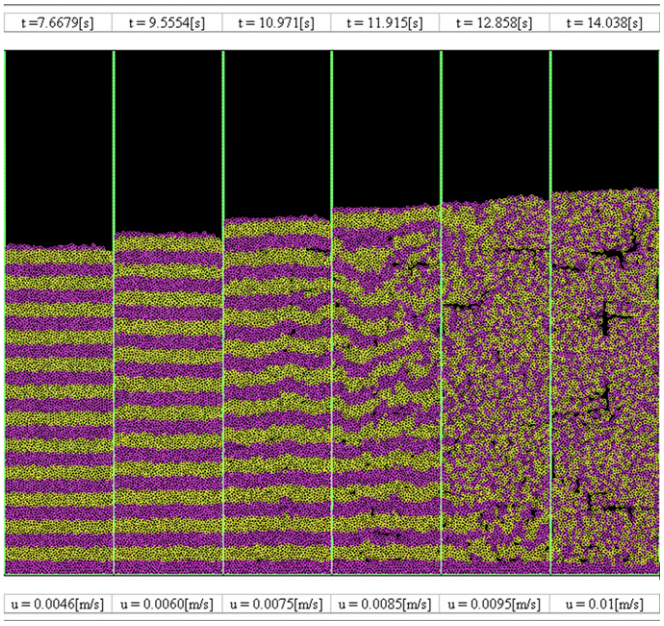

Fig. 5. Sequential snapshots of bed expansion with increasing gas velocity ($K=1$).

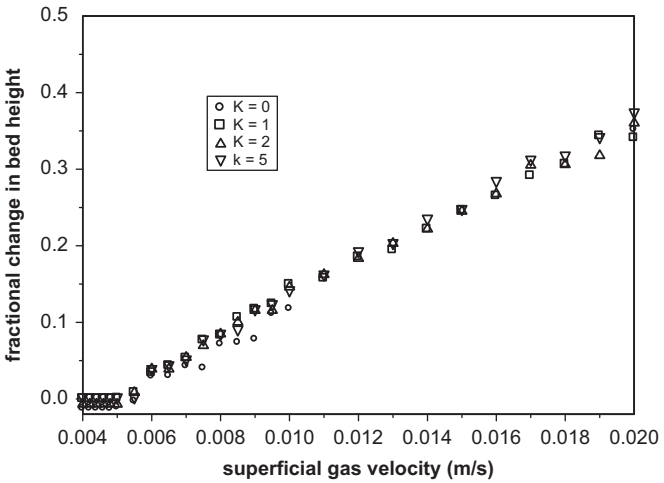

Fig. 7. Effect of surface energy on bed expansion.

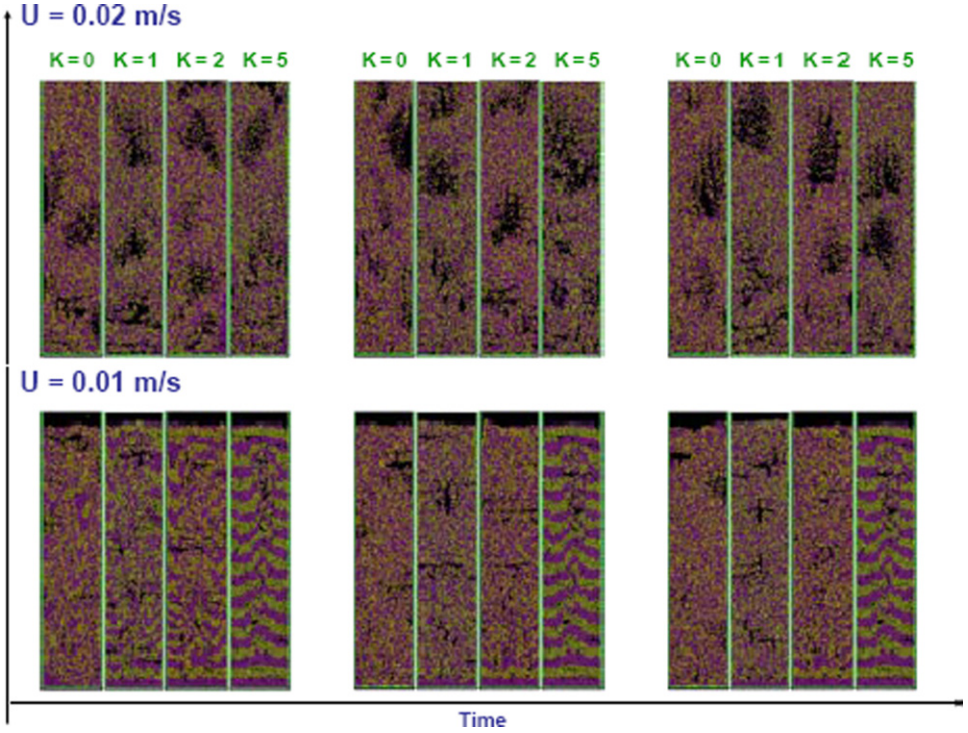

Fig. 6. Typical snapshots of the bed for gas velocities of 0.01 m/s and 0.02 m/s and $K=0$, 1, 2 and 5.

lies in the range 0.01 m/s $\leq U_{mb} \leq$ 0.02 m/s and that with increasing surface energy a higher gas velocity is required to reach the bubbling regime, if that is possible. These are similar results to those obtained by Ye et al. (2004) who used a 2D DEM–CFD model to study the interparticle force effect on Group A fluidisation and found that the minimum bubbling velocity U_{mb}, based on the observation of the first appearance of a bubble in the bed, increased with increase in surface energy. They also observed that channelling occurred for higher surface energies.

Fig. 7 indicates that the rate of bed expansion with increasing gas velocity is essentially the same for all cases, although the initial bed expansion for 0.005 m/s $< U <$ 0.01 m/s is slightly lower when $K=0$. Some researchers have reported a decrease in the bed height near the minimum bubbling point U_{mb}. However this pheno-menon is not observed in our simulations.

Fig. 8 shows the effect of surface energy on the evolution with increasing superficial gas velocity of the pressure drop and the average number of contacts. It can be seen that in the fixed bed regime the pressure drop curve is independent of surface energy. A pressure drop overshoot occurs around the minimum fluidisation velocity for the systems with surface energy. For $K=1$ and $K=2$ the overshoot is slight but, for $K=5$, the average pressure drop increases to a maximum value that is 10% greater than that necessary to balance the self-weight of the bed and then drops to equal the bed weight divided by the cross-sectional area of the bed. To understand the overshoot phenomenon, a bed with vertical periodic boundaries was simulated. The data indicate that the overshoot is solely due to the wall effect; this is considered further below. Therefore for all the cases with $K > 0$, minimum fluidisation occurs when the normalized pressure drop first equals unity, which occurs before the overshoot appears.

The most notable aspect of Fig. 8 is that, for $K > 0$, bond breaking occurs in two stages: (i) approximately 40% of bonds are broken, creating a 'partially fluidised' bed, and (ii) for a higher bond strength a higher gas velocity is required to break the remaining bonds in order to 'fully fluidise' the bed. Fig. 9 illustrates the effect of surface energy on the loss of interparticle contacts in the bed and the corresponding increase in the proportion of "fines" as the gas velocity is increased in the 'homogeneous expansion' regime. For convenience, fines are here defined as singlets, doublets and triplets. It can be seen that no more than 10% of fines are produced until the gas velocity is high enough to reduce the number of contacts to below 60% of the original number. Initially, in the fixed bed regime all of the particles are interconnected in one big cluster/agglomerate. For

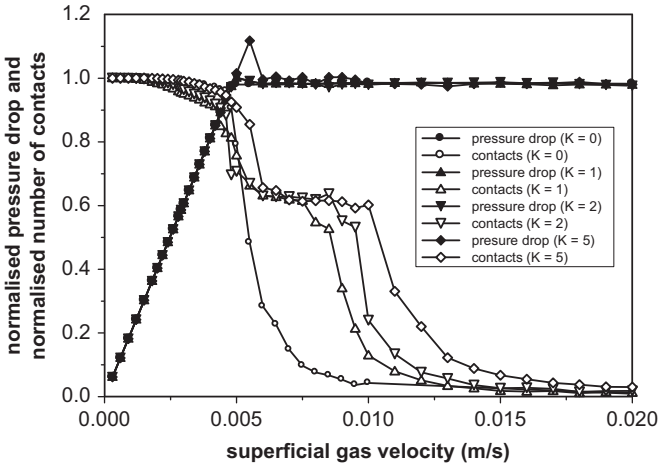

Fig. 8. Effect of surface energy on the evolution of pressure drop and number of contacts with increasing superficial gas velocity.

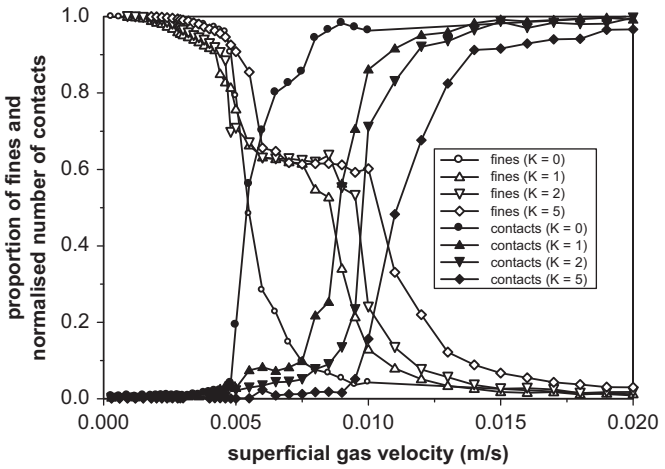

Fig. 9. Breakup of the connectivity network.

Table 5
Minimum fluidisation and minimum bubbling velocities for $K=0$, 1, 2 and 5.

	$K=0$	$K=1$	$K=2$	$K=5$
U_{mf} (m/s)	0.0048	0.0048	0.0048	0.0048
U_{mb} (m/s)	0.01	0.014	0.015	0.02
U_{mb}/U_{mf} (dimensionless)	2.08	2.92	3.12	4.17

$K > 0$, when the gas velocity is increased above U_{mf}, a sufficient number of contacts is broken to form a few relatively large agglomerates, which consist of most of the particles in the bed, and the proportion of singlets, doublets and triplets is small. The strength of the agglomerates so formed depends on the strength of the interparticle bonds. As can be seen in Fig. 9, further bond breaking required to fracture the initially formed agglomerates requires a higher gas velocity for higher values of surface energy. Once this has been achieved, further disintegration of the agglomerates continues progressively until the fines predominate and occupy the whole bed. At this point the bed can be considered to be 'fully fluidised'.

On this basis, minimum fluidisation and minimum bubbling velocities for the cases with and without surface energy are shown in Table 5. Fig. 10 shows typical particle configurations when $K=0$, 1, 2 and 5 for gas velocities of 0.01 m/s, 0.014 m/s, 0.015 m/s and 0.02 m/s, corresponding to the minimum bubbling velocities given in Table 5.

The snapshots shown in Fig. 11 illustrate the evolution of the structure of the particle bed as the superficial gas velocity is increased from below the minimum fluidised velocity U_{mf} to the minimum bubbling velocity U_{mb} step by step, for $K=0$. In each snapshot, the three columns show (i) the six largest cluster sizes in the system (left column), (ii) singlets, doublets and triplets (centre column; colour coded by size) and (iii) the spatial distribution of interparticle contacts (right column). Note that clusters of intermediate sizes are not shown. It can be seen that the number of interparticle contacts decreases sharply when U_{mf} is reached and correspondingly the mass percentage of singlets, doublets and triplets increases sharply. The figure clearly shows the degradation of large clusters, the increase in fines production and the corresponding loss of contacts as the gas velocity is increased.

In the fixed bed regime, as shown in the snapshots for $U=0.0048$ m/s, almost all of the particles belong to one big cluster. When $U=0.0050$ m/s the big cluster has broken into

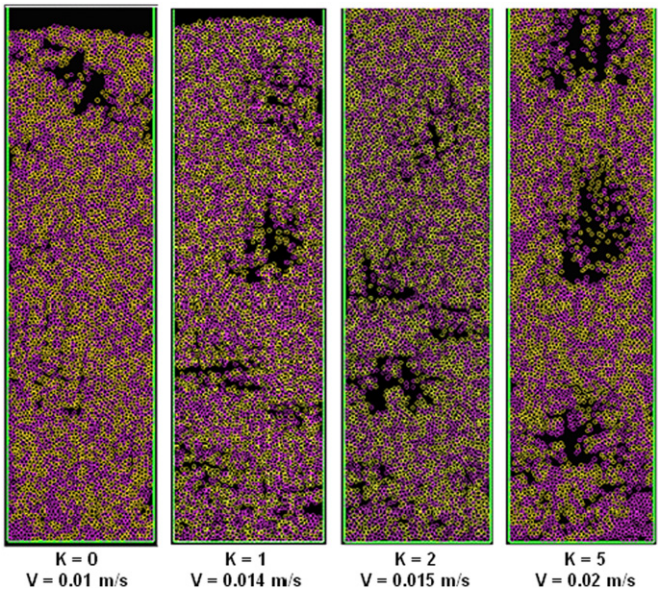

Fig. 10. Typical particle configurations when $K=0$, 1, 2 and 5 for gas velocities of 0.01 m/s, 0.014 m/s, 0.015 m/s and 0.02 m/s.

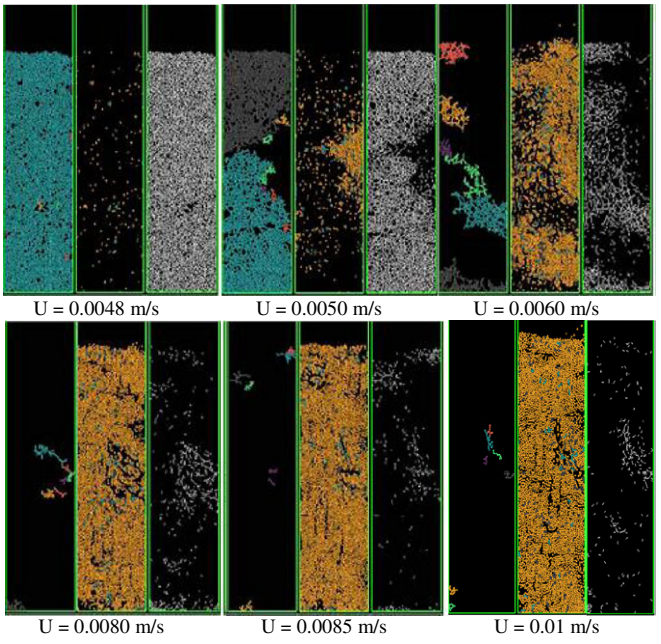

Fig. 11. Cluster visualisation when $K=0$.

two large clusters with a significant increase in the number of singlets, doublets and triplets. Note that, at $U=0.0050$ m/s, the two very large clusters (shown in blue and dark grey) are not connected to each other. In other words, the particle connectivity between the bottom and the top of the bed has been broken. By further increasing the gas velocity, the cluster sizes continuously decrease until the bed is full of singlets, doublets and triplets, at which stage the number of remaining contacts is very small.

Fig. 12 illustrates the evolution of the bed structure for $K=1$. Initially, the structure of the bed breaks into two when minimum fluidisation is reached. The difference from the $K=0$ case is that, due to surface energy, there are two agglomerates rather than two clusters and consequently the number of singlets, doublets and triplets remains low until $U=0.0075$ m/s. At this point, the second large reduction in the number of contacts begins

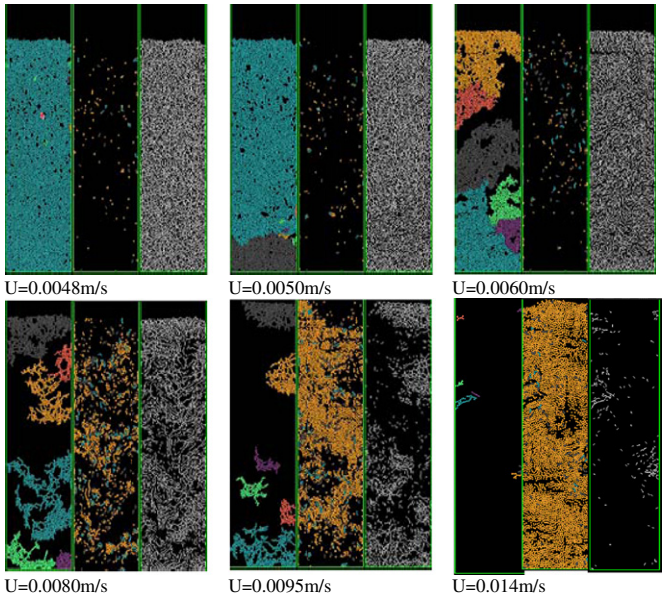

Fig. 12. Cluster visualisation when $K=1$.

(see Fig. 8) when the gas velocity is sufficiently high to break up the large agglomerates, leading to a corresponding rapid increase in the fractional mass of fine particles, as shown in Fig. 9. With further increase in gas velocity, the connectivity network completely disintegrates until finally the bed consists entirely of singlets, doublets and triplets and is fully fluidised.

4. Discussion

The results of the simulations reported in Section 3 indicate that the value of U_{mf} is independent of the value of surface energy used. However, this result needs to be qualified. In the simulations the value of surface energy was attributed to the particles after pluvial deposition of the particle bed. It can be argued that it would be more realistic to introduce surface energy prior to pluvial deposition when the system is in the state of a granular gas with no contacts. The consequence of this would be that the initial voidage of the packed bed would be expected to be higher and this in itself would affect the value of U_{mf}. The significance of the results reported in this paper is that although, in reality, the value of U_{mf} may depend on the value of surface energy this is solely due to the higher voidage of the initial bed and not to increased bed resistance resulting from stronger interparticle bonds.

Rhodes et al. (2000) investigated the transition from freely bubbling to cohesive behaviour when a superficial velocity of 0.64 m/s was applied to a 2D monodisperse bed of 8000 spheres ($d_p=500$ μm, $\rho_p=2650$ kg/m^3). An artificially imposed (constant) interparticle attractive force was used which was a multiple, K, of the single particle buoyant weight. From the analysis of snapshots of the beds, obtained for a wide range of K values, it was deduced that the onset of cohesive behaviour occurred when $K=47$. When the particle size was doubled it was found that the corresponding value of K was 16. In a later paper, Wang and Rhodes (2004) used a larger bed (15,000 spheres) and concluded that $K=30$ represents a typical condition of defluidisation. A state of complete defluidisation, i.e. negligible bed activity, was observed when K was increased to about 40.

Xu et al. (2001) examined the effect of interparticle adhesive forces on fluidisation behaviour using a monodisperse system of 4500 spheres ($d_p=100$ μm, $\rho_p=1440$ kg/m^3). They used a van der

Waals force of 8.76×10^{-8} N, corresponding to a Hamaker constant of 2.1×10^{-20} J, which for the particles they considered is equivalent to a value of $K=12$. From their simulations they found $U_{mf}=0.012$ m/s and $U_{mb}=0.028$ m/s. Then, using a superficial velocity $U=0.048$ m/s, they examined the effect of artificially increasing the van der Waals forces by changing K. From snapshots of the beds, they concluded that good fluidisation was obtained with continuous bubbles of relatively small size rising through the bed if $K<30$. For $40<K<100$, the fluidisation quality deteriorated significantly and severe channelling occurred, although the bed was fluidisable at higher gas velocities. When $K>300$, fluidisation was impossible with the bed consisting of large blocks of particles.

Ye et al. (2004) simulated a fluidised bed consisting of monodisperse spheres ($d_p=100$ μm, $\rho_p=900$ kg/m^3) and calculated the van der Waals forces based on Hamaker constants of 10^{-22}, $10^{-21}$and 10^{-20} J, which for their particles correspond to values of $K=0.56$, 5.6 and 56. In all three cases, U_{mf} was found to be about 0.004 m/s. Snapshots of the beds indicated that $U_{mb}=$ 0.028 m/s and 0.030 m/s for $K=0.56$ and 5.6 respectively. For $K=56$, however, no obvious bubble appeared when $U=0.052$ m/s but channelling was observed adjacent to the side walls.

Moreno-Atanasio et al. (2007) simulated monodisperse 2D fluidised beds consisting of 45,000, 98 μm-sized spheres. They used Eq. (5) to calculate the force required to break an adhesive contact for values of surface energy equal to 0.37 mJ/m^2 and 37 mJ/m^2 which, for their particle system, corresponds to values of $K=6.8$ and 68 respectively. These authors, however, did not use JKR theory to model the particle–particle interactions. Instead, they used the conventional linear spring-dashpot model and simply added the 'adhesion force' to the spring and dashpot forces in the equation of motion, when particles were in contact.

It was shown in Fig. 6 that, when the superficial gas velocity was 0.01 m/s, channelling occurred if $K=5$. This value is much lower than the values quoted by the above authors. However, it is noted that all the above authors simply include the adhesion force in the equations of motion when a contact is first established. When two particles are separating, the adhesion force is set to zero when the contact overlap $\alpha\leq0$. The above authors also assume that adhesion has no effect on the repulsive normal force–displacement relationship. Consequently, for the case of a linear spring model, the resultant (effective) normal contact force–displacement relationship is as illustrated in Fig. 13a. As shown in the figure, when contact is first made ($\alpha=0$) the effective normal force is equal to the adhesion force indicated by point A. The line 0A illustrates the 'jump to contact' observed in AFM experiments. When the two particles are compressed the effective normal force increases along line AB, which is parallel to the repulsive force–displacement line given by $P=k_n\alpha$. During unloading the force decreases along line BA, and at point A, when $\alpha=0$, all the elastic work done during loading has been recovered. In the simulations reported by the above authors the adhesion force is set to zero and the force instantaneously follows the line A0. This is physically unrealistic since it implies that a contact 'bond' can be broken without doing any work.

In contrast, the JKR model of adhesion, as illustrated in Fig. 13b, modifies the repulsive Hertzian contact force–displacement relationship and requires extra work to be done in order to break the contact. As shown in the figure, there is a 'jump to contact', i.e. OA, when $\alpha=0$. During compressive loading and unloading the force follows the path ABA. On returning to point A all the elastic work done during loading has been recovered but the radius of the contact area is finite at point A. If the contact is to be broken the force has to follow the curve AC. At point C the contact breaks, the force instantaneously becomes zero and the work required to break the contact W_c is given by the area under the curve AC;

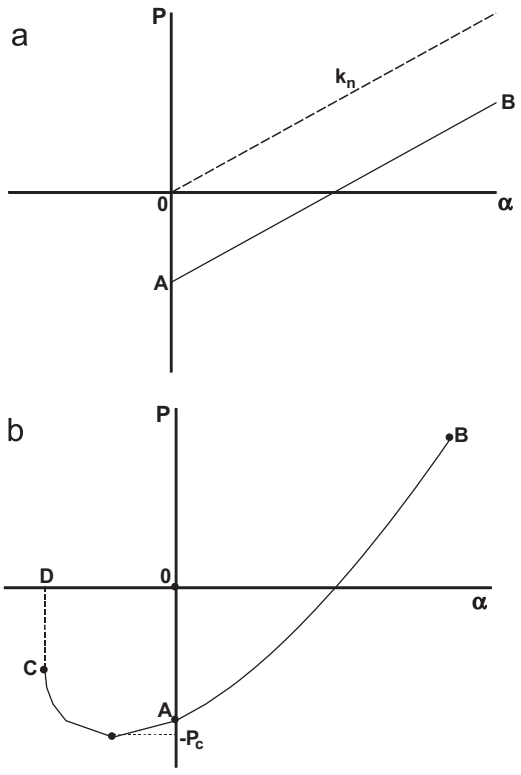

Fig. 13. Normal contact force–displacement relationships: (a) linear spring plus adhesion force model (b) JKR model.

which can be expressed (Thornton and Ning, 1998) as

$$W_c=7.09\left(\frac{\Gamma^5R^{*4}}{E^{*2}}\right)^{1/3} \tag{10}$$

If the adhesion force is simply included in the equations of motion and set to zero when $\alpha\leq0$, no work is required to break a contact. In simulations using this approach it is difficult to prevent contacts breaking unless an excessively high value is attributed to the adhesion force. Consequently, the values of K reported by the above authors are physically unrealistic.

The question remains as to the physical basis for the apparently homogeneous expansion which is a characteristic feature of beds of Group A particles. As discussed earlier, stability analyses for uniform fluidised beds predict that they will not be stable against voidage perturbations so that if this approach is taken, some form of elasticity of the bed must be invoked, either deriving from the elastic behaviour of particle contacts (Rietema and co-workers) and/or hydrodynamic factors (Gibilaro and co-workers). However in the simulations for both $K=0$ and $K=1$, when $U=0.0050$ m/s, the connectivity from the bottom to the top of the bed has been broken. Consequently, the bed expansion cannot be attributed to the so-called elasticity of the bed structure.

Foscolo and Gibilaro (1984) proposed a hydrodynamic criterion to predict the onset of bubbling in fluidised beds. Their approach was based on the suggestion of Wallis (1969) that bubbles occur when the propagation velocity of a voidage disturbance, u_ε, reaches the velocity of elastic waves, u_e, in the bed. From the criterion that $u_\varepsilon=u_e$ they obtained a prediction of the voidage at minimum bubbling velocity U_{mb}. However, their model implies that U_{mb} is independent of surface energy. In a subsequent paper (Foscolo et al., 1985) they attempted to incorporate interparticle (adhesive) forces into their model and as a consequence purported to show that when $u_\varepsilon=u_e$ the voidage

and hence U_{mb} increases with increase in the so-called interparticle force. This result was obtained by adding an extra term in the equation for the elastic wave velocity that accounted for the so-called interparticle force. Their argument, however, is flawed by the fact that their interparticle force term is related to the so-called elasticity of the bed, as suggested by Rietema (1973). The simulation results shown in Fig. 12 demonstrate that, for adhesive particles, the bed starts to break-up into agglomerates as soon as U_{mf} is exceeded and that the agglomerates disintegrate with further increases in the superficial gas velocity. Consequently, the simulations demonstrate that the modified theory of Foscolo et al. (1985) is not applicable to beds of adhesive particles, irrespective of the type of adhesion, *i.e.* van der Waals, electrostatic, magnetic or liquid bridge forces.

A further difficulty for theories based on stability of continuous structures is illustrated by the results for $K=1$ in Fig. 12. From the simulations, there is a cluster at the top of the bed, the top of which defines the bed height and the bed height increases incrementally as the gas velocity is incrementally increased. Therefore the bed expansion is simply due to the increased gas velocity 'lifting' the uppermost cluster to a higher position. It is also clear from Fig. 12 that the expansion of the bed is not homogeneous due to the existence of agglomerates in which the particles are moving in unison with each other. In other words, the strain in an agglomerate is negligible compared to the apparent strain suggested by the movement of the top of the bed.

Massimilla and co-workers have a different view of the expanded bed, derived from direct microscopic observation, in which the structure does not expand uniformly, at least not on a single particle level, but by nucleation and growth of cavities. They draw attention to the role of such cavities in focussing the through-flow of gas, which as the gas flow increases, causes the cavities to expand. This is in agreement with the findings of the present simulations, which also show cavity formation and expansion. Their studies clearly could not show the existence of agglomerates or the lack of continuity in the structure. It was also observed by Geldart and Wong (1984) that Group A powders 'are far from being homogeneous'.

A further piece of evidence that aggregates occur in fluidised beds of particles under the influence of van der Waals forces alone can be found in the results of experiments on fine particles — in Geldart's group *C*. In this case, fluidisation often does not take place at all, but if it does occur, sometimes induced by applied vibration, it does so with the particles in aggregated form (see, for example, Chaouki et al., 1985; Lauga et al., 1991; Wang et al., 2002). The resulting aggregates are sometimes strong enough to be removed intact from the bed. It is well-known, of course, that with the addition of stronger interparticle forces by the addition of free liquid to the bed, strong aggregation can occur, and this effect is exploited in commercial fluidised bed agglomerators.

5. Stability considerations

Consider a 2D system of spheres and assume a coefficient of interparticle friction $\mu=\infty$ (no sliding anywhere). The number of degrees of freedom for a single particle is 3 (two linear velocities and one rotational velocity). Therefore if the number of particles is N the total number of degrees of freedom for the system is $3N$. The number of unknown forces (constraints) at a contact is 2 (one normal force and one tangential force) and if there is C number of contacts then the total number of unknown forces in the system is $2C$. If the total number of degrees of freedom equals the total number of constraints then the system (structure) is said to be deterministic (isostatic). In this case

$$3N=2C \text{ or } C/N=3/2 \tag{11}$$

For this condition we can define a critical coordination number (average number of contacts per particle) as

$$Z_c=2C/N=3 \tag{12}$$

If $Z>Z_c$ then the system is indeterminate (hypostatic) which means there are more contacts than necessary to ensure stability. It is a redundant system. If $Z<Z_c$ then equilibrium cannot be satisfied which means there are fewer contacts than necessary to keep the system stable and the system becomes a mechanism (hyperstatic).

Defining the coordination number as $Z=2C/N$ is not appropriate since this is the apparent coordination number and includes particles

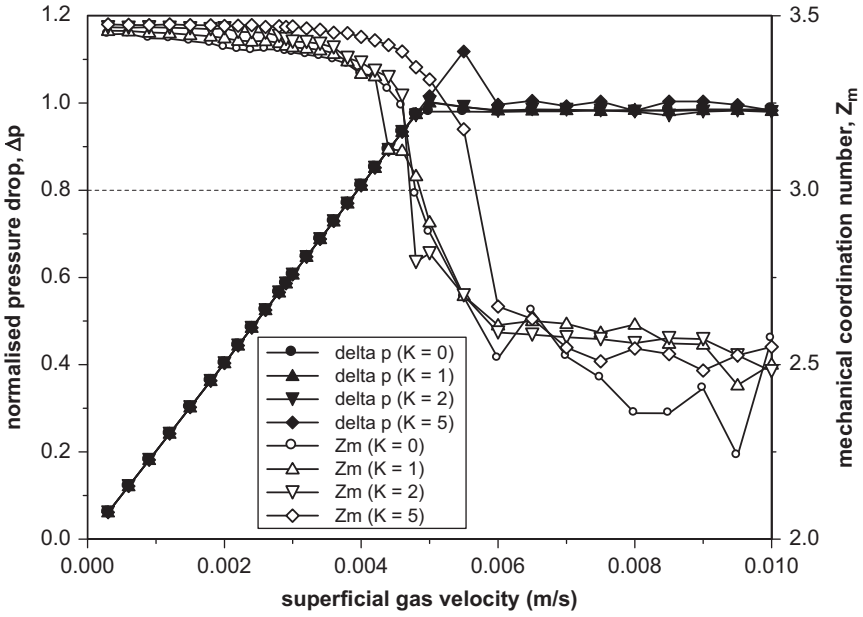

Fig. 14. Evolution of the average pressure drop and the average mechanical coordination number with increasing gas velocity for a wall bounded system when the surface energy is such that $K=0$, 1, 2 and 5.

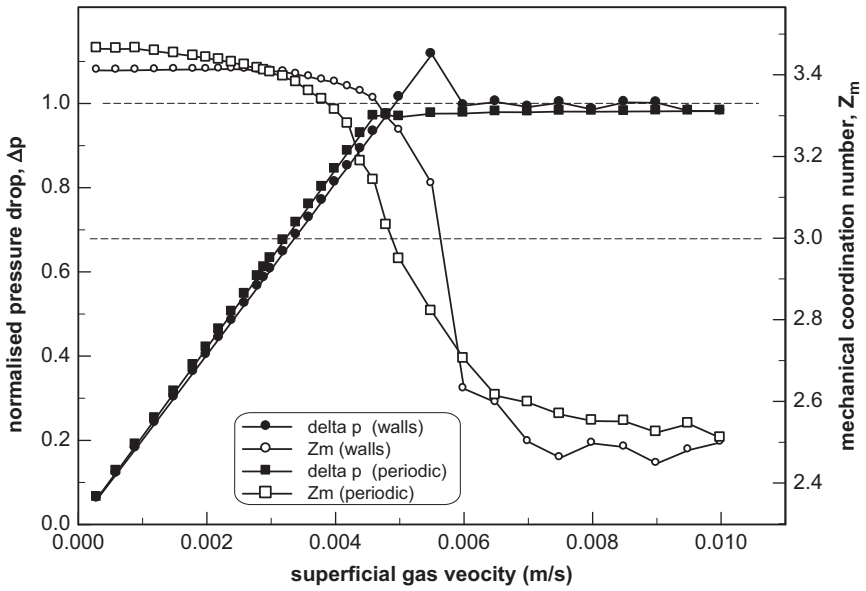

Fig. 15. Evolution of the average pressure drop and the average mechanical coordination number with increasing gas velocity for a wall bounded system and a system with vertical periodic boundaries when the surface energy is such that $K=5$.

with no contacts. We can define a geometric coordination number

$$Z_g = 2C/(N-N_0) \tag{13}$$

where N_0 is the number of particles with no contacts. However, this definition includes particles with only one contact and these do not contribute to the stability of the system. Therefore, in order to examine stability, we define a mechanical coordination number

$$Z_m = (2C-N_1)/(N-N_1-N_0) \tag{14}$$

where N_1 is the number of particles with only one contact.

In Fig. 14, the average pressure drop and the average mechanical coordination number are plotted against superficial gas velocity for different values of K. The figure indicates that $Z_m \sim 3$ when $U \sim U_{mf}$, except for the case of $K=5$. Fig. 15 shows the effect of increasing the gas velocity on the normalised pressure drop and the mechanical coordination number for $K=5$. The figure shows results obtained for both a wall bounded system and a system with vertical periodic boundaries. It can be seen from Fig. 15 that when the average pressure drop becomes equal to the bed weight divided by the cross-sectional area of the bed (for the case of vertical periodic boundaries) and when, in the case of a wall bounded system, the overshoot in the average pressure drop reaches a maximum value then the mechanical coordination number $Z_m \sim 3.15$. For systems with finite values of interparticle friction (in this case $\mu=0.3$) the stability criterion is uncertain but is expected to be somewhat higher than 3 (in 2D $Z_c=3$ for $\mu=\infty$). Therefore, it is concluded that U_{mf} corresponds to the point when the system becomes hyperstatic, signifying the start of a transition from solid-like to fluid-like behaviour.

Pandit et al. (2006) explained that the reason for an overshoot in the bed pressure drop curve is the time taken by the bed particles to rearrange themselves in response to the increment given to the gas velocity. They also argued that, in the presence of cohesive interparticle forces, the bed particles take a longer time to rearrange themselves and this leads to the overshoot in the bed pressure drop curve. Ye et al. (2004) reported that the generation of the overshoot of the pressure drop near the minimum fluidisation point is affected by both the particle-wall friction and the interparticle van der Waals forces. However, as demonstrated by Fig. 15, when vertical periodic boundaries are used there is no overshoot in the pressure drop, clearly indicating that, at least for the simulations presented here, the pressure drop overshoot is an artefact resulting from the extra kinematic constraint provided by the wall boundaries.

6. Conclusions

Results have been presented to show how the pressure drop, bed expansion, number of contacts and average coordination number change with superficial gas velocity. Visualisations, including video sequences, have been used to illustrate how the particle configuration, the particle velocity field, the fluid velocity field and the spatial distribution of interparticle contacts vary as the superficial gas velocity is increased.

The results of the simulations presented indicate that $U=U_{mf}$ when the fluid pressure drop across the bed first equals the buoyant weight of the solid particles per unit cross-sectional area. This occurs before any apparent overshoot. For adhesive particle systems, the simulations indicate that the pressure drop overshoot is an artefact due to the constraint provided by the vertical wall boundaries.

Because surface energy was introduced after pluvial deposition of the bed, the value of U_{mf} was found to be independent of the value of surface energy used. This demonstrates that surface energy dependency of U_{mf} in real experiments is due to differences in initial bed voidage and is not due to increased bed resistance resulting from stronger interparticle bonds.

At U_{mf} the system is not fully fluidised in that U_{mf} corresponds to the point when the system becomes a mechanism. When surface energy is introduced to the system, the bed breaks up into large agglomerates at minimum fluidisation and in order to break down these agglomerates to create a fully fluidised bed, higher superficial gas velocities are required as the value of surface energy is increased.

For $U > U_{mf}$ the connectivity between the bottom of the bed and the top surface no longer exists and the bed expansion is not homogeneous. Consequently, Rietema's (1973) suggestion that the bed expansion is due to the bed 'elasticity' is not tenable. If we define a 'fully fluidised' bed as one in which the 'particles' consist

of only singlets, doublets and triplets that occupy the whole bed then, as the surface energy is increased, a higher gas velocity is required to attain this 'fully fluidised state'. The fully fluidised state corresponds to U_{mb} and only when this state has been reached can bubbling occur. Minimum bubbling velocity U_{mb} increases with surface energy.Therefore, with increasing surface energy, the so-called 'homogeneous' expansion regime is extended. Once the bed is fully fluidised the effect of surface energy is no longer significant.

Acknowledgement

The work reported above was part of a project supported by an EPSRC Grant (No. GR/T17076/01).

References

Abrahamsen, A.R., Geldart, D., 1980. behaviourof gas-fluidized beds of fine powders. Part I. Homogeneous expansion. Powder Technol. 26, 35–46.
Chaouki, J., Chavarie, C., Klvana, D., Pajonk, G., 1985. Effect of interparticle forces on the hydrodynamic behaviour of fluidized aerogels. Powder Technol. 43, 117–125.
Di Felice, R., 1994. The voidage function for fluid particle interaction systems. Int. J. Multiphase Flow 20, 153–159.
Di Renzo, A., Di Maio, F.P., 2007. Homogeneous and bubbling fluidisation regimes in DEM–CFD simulations: hydrodynamic stability of gas and liquid fluidized beds. Chem. Eng. Sci. 62, 116–130.
Donsi, G., Massimilla, L., 1973. Bubble-free expansion of gas-fluidized beds of fine particles. AIChE J. 19, 1104–1110.
Ergun, S., 1952. Fluid flow through packed columns. Chem. Eng. Prog. 48, 89–94.
Foscolo, P.U., Gibilaro, L.G., 1984. A fully predictive criterion for the transition between particulate and aggregate fluidisation. Chem. Eng. Sci. 39, 1667–1675.
Foscolo, P.U., Gibilaro, L.G., Di Felice, R., Waldram, S.P., 1985. The effect of interparticle forces on the stability of fluidized beds. Chem. Eng. Sci. 40, 2379–2381.
Geldart, D., 1973. Types of gas fluidisation. Powder Technol. 7, 285–292.
Geldart, D., 1986. Gas Fluidisation Technology. Wiley, Chichester.
Geldart, D., Wong, A.C.Y., 1984. Fluidisation of powders showing degrees of cohesiveness—I. Bed expansion. Chem. Eng. Sci. 39, 1481–1488.
Helland, E., Occelli, R., Tadrist, L., 2000. Numerical study of cluster formation in a gas-particle circulating fluidised bed. Powder Technol. 110, 210–221.
Hilton, J.E., Mason, L.R., Cleary, P.W., 2010. Dynamics of gas–solid fluidised beds with non-spherical particle geometry. Chem. Eng. Sci. 65, 1584–1596.
Hoomans, B.P.B., Kuipers, J.A.M., Briels, W.J., Van Swaaij, W.P.M., 1996. Discrete particle simulation of bubble and slug formation in a two-dimensional gas-fluidised bed: a hard-sphere approach. Chem. Eng. Sci. 51, 99–118.
Jackson, R., 1963. The mechanics of fluidised beds: part I: the stability of the state of uniform fluidisation. Trans. IChemE 41, 13–21.
Johnson, K.L., Kendall, K., Roberts, A.D., 1971. Surface energy and the contact of elastic solids. Proc. R. Soc. London A 324, 301–313.
Kafui, K.D., Thornton, C., Adams, M.J., 2002. Discrete particle-continuum fluid modelling of gas-solid fluidised beds. Chem. Eng. Sci. 57, 2395–2410.
Kafui, D.K., Johnson, S., Thornton, C., Seville, J.P.K., 2011. Parallelization of a Lagrangian–Eulerian DEM/CFD code for application to fluidized beds. Powder Technol. 207, 270–278.
Kaneko, Y., Shiojima, T., Horio, M., 1999. DEM simulation of fluidized beds for gas-phase olefin polymerization. Chem. Eng. Sci. 54, 5809–5821.
Kawaguchi, T., Sakamoto, M., Tanaka, T., Tsuji, Y., 2000. Quasi-three-dimensional numerical simulation of spouted beds in cylinder. Powder Technol. 109, 3–12.
Lauga, C., Chaouki, J, Klvana, D., Chavarie, C., 1991. Improvement of the fluidisability of Ni/SiO_2 aerogels by reducing interparticle forces. Powder Technol. 65, 461–468.
Molerus, O., 1982. Interpretation of Geldart's Type A, B, C and D powders by taking into account interparticle cohesion forces. Powder Technol. 33, 81–87.
Moreno-Atanasio, R., Xu, B.H., Ghadiri, M., 2007. Computer simulation of the effect of contact stiffness and adhesion on the fluidisation behaviour of powders. Chem. Eng. Sci. 62, 184–194.
Pandit, J.K., Wang, X.S., Rhodes, M.J., 2006. On Geldart Group A behaviour in fluidized beds with and without cohesive interparticle forces: a DEM study. Powder Technol. 164, 130–138.
Rhodes, M.J., Wang, X.S., Nguyen, M., Liffman, K., 2000. The influence of interparticle forces on fluidized bed behaviour. In: Flamant, G., Gauthier, D., Hemeh, M., Steinmetz, D., (Eds.), Proceedings of the 3rd European Conference on Fluidisation, Toulouse, France, pp 543–550.
Rhodes, M.J., Wang, X.S., Nguyen, M., Stewart, P., Liffman, K., 2001a. Use of discrete element method simulation in studying fluidisation characteristics: influence of interparticle force. Chem. Eng. Sci. 56, 69–76.
Rhodes, M.J., Wang, X.S., Nguyen, M., Stewart, P., Liffman, K., 2001b. Study of mixing in gas-fluidized beds using a DEM model. Chem. Eng. Sci. 56, 2859–2866.
Rietema, K., 1973. The effect of interparticle forces on the expansion of a homogeneous gas-fluidised bed. Chem. Eng. Sci. 28, 1493–1497.
Rietema, K., Cottaar, E.J.E., Piepers, H.W., 1993. The effects of interparticle forces on the stability of gas-fluidized beds—II. Theoretical derivation of bed elasticity on the basis of van der Waals forces between powder particles. Chem. Eng. Sci. 48, 1687–1697.
Seville, J.P.K., Willett, C.D., Knight, P.C., 2000. Interparticle forces in fluidisation: a review. Powder Technol. 113, 261–268.
Takeuchi, S., Wang, S., Rhodes, M., 2004. Discrete element simulation of a flat-bottomed spouted bed in the 3-D cylindrical coordinate system. Chem. Eng. Sci. 59, 3495–3504.
Thornton, C., Yin, K.K., 1991. Impact of elastic spheres with and without adhesion. Powder Technol. 65, 113–123.
Thornton, C., Kafui, D., 2002. 3D DEM simulations of gas–solid fluidised beds. In: Cook, B.K., Jensen, R.P., (Eds.), Proceedings of the 3rd International Conference on Discrete Element Methods, ASCE Geotechnical Special Publication, vol. 117, pp. 178–182.
Thornton, C., Ning, Z., 1998. A theoretical model for the stick/bounce behaviour of adhesive, elastic-plastic spheres. Powder Technol. 99, 154–162.
Tsuji, Y., Kawaguchi, T., Tanaka, T., 1993. Discrete particle simulation of two-dimensional fluidized bed. Powder Technol. 77, 79–87.
Tsuji, T., Yabumoto, K., Tanaka, T., 2008. Spontaneous structures in three-dimensional bubbling gas-fluidized bed by parallel DEM–CFD coupling simulation. Powder Technol. 184, 132–140.
Wallis, G.B., 1969. One-dimensional Two-phase Flow. McGraw-Hill, New York.
Wang, X.S., Rhodes, M.J., 2004. Mechanistic study of defluidization by numerical simulation. Chem. Eng. Sci. 59, 215–222.
Wang, Y., Gu, G., Wei, F., Wu, J., 2002. Fluidisation and agglomerate structure of SiO_2 nanoparticles. Powder Technol. 124, 152–159.
Xu, B.H., Yu, A.B., 1997. Numerical simulation of the gas–solid flow in a fluidised bed by combining discrete particle method with computational fluid dynamics. Chem. Eng. Sci. 52, 2785–2809.
Xu, B.H., Yu, A.B., Zulli, P., 2001. The effect of interparticle forces on powder fluidisation behaviour. In: Kishino, Y. (Ed.), Powders and Grains 2001. Swets & Zeitlinger, Lisse, pp. 577–580.
Ye, M., Van der Hoef, M.A., Kuipers, J.A.M., 2004. A numerical study of fluidisation behaviour of Geldart A particles using a discrete particle code. Powder Technol. 139, 129–139.
Yuu, S., Nishikawa, H., Umekage, T., 2001. Numerical simulation of air and particle motions in group-B particle turbulent fluidized bed. Powder Technol. 118, 32–44.